Article

Sedimentary Environment and Model for Organic Matter Enrichment: Chang 7 Shale of Late Triassic Yanchang Formation, Southern Margin of Ordos Basin, China

Yonggang Zhao [1,2], Chunyu Zhang [3,4], Jungang Lu [3,4,*], Xingcheng Zhu [3,4], Lei Li [5] and Shanghua Si [1,2]

1   School of Earth Sciences and Engineering, Xi'an Shiyou University, Xi'an 710065, China;
    ygzh@xsyu.edu.cn (Y.Z.); sishanghua0724@163.com (S.S.)
2   Shaanxi Key Laboratory of Petroleum Accumulation Geology, Xi'an Shiyou University,
    Xi'an 710065, China
3   Natural Gas Geology Key Laboratory of Sichuan Province, Southwest Petroleum University,
    Chengdu 610500, China; zcy1_cq@petrochina.com.cn (C.Z.); zhuxingcheng_j@163.com (X.Z.)
4   School of Geoscience and Technology, Southwest Petroleum University, Chengdu 610500, China
5   College of Geosciences, China University of Petroleum, Beijing 102249, China;
    2020310001@student.cup.edu.cn
*   Correspondence: lujungang21@aliyun.com

Abstract: Shale oil is an unconventional oil resource that needs to be developed and utilized urgently. However, the Chang 7 shale in the Ordos Basin, as the most typical continental source rock in China, is limited by the study of organic matter (OM) enrichment factors in continental lacustrine facies, and there are still controversies about the controlling factors, which limit the progress of oil and gas exploration. This paper aims to reconstruct the paleoenvironment of Chang 7 shale in the southern margin of Ordos Basin and reveal the controlling factors of organic rich shale by organic and elemental analysis, X-ray diffraction (XRD) analysis, thin section observation, and scanning electron microscopy-energy dispersive spectrometer (SEM-EDS) analysis. The results show that during the deposition period of Chang 7 shale, the climate was warm and humid, the lake water has strong reducing, low salinity and rapid depth changes. Total organic carbon (TOC) is positively correlated with salinity and hydrothermal action and inversely proportional to terrigenous input. The high productivity, low consumption and low dilution result in high enrichment of shale OM in the southern margin of Ordos Basin.

Keywords: lacustrine shale; organic matter enrichment; Late Triassic; Chang 7; southern margin of Ordos Basin

1. Introduction

Shale is widely known in nature, accounting for about 55% of the distribution area of sedimentary rocks [1]. Organic-rich black shale is the main rock type to form shale oil and gas. Shale can be formed in three types of sedimentary environments (marine facies, transitional facies of marine and continent and lacustrine facies) [2–5]. The formation of organic-rich black shale requires two important conditions: the development of plankton in surface waters and high productivity [6,7], and it has the conditions conducive to the preservation, accumulation and transformation of sedimentary rock organic matter (OM) [8,9]. Various sedimentary models are used to summarize the formation mechanism of black shale: silled-basin model or modified silled-basin model [10], upwelling model [11], oxygen-minimum zone model [11], model of an oxygen minimum zone (OMZ) in a shelf sea [12,13], silled-basin transgressive chemocline model [14], photic zone euxinia model [15] and estuarine circulation nutrient model [16]. The terrestrial lacustrine basin has limited sedimentary water, and the water circulation capacity is less than that of the ocean, so that the rich-organic black shale mainly develops in two depositional models (water

stratification and lake transgression) [17,18]. These sedimentary models are an important basis for the understanding of OM enrichment of shale. OM hosted pores are the most prevalent pores in organic-rich shale, in which shale gas is generated and stored [19–21].

According to the sedimentary environment, terrestrial organic black shale can be divided into three categories in China: (1) organic black shale of marine facies, (2) rich-organic black shale of transitional facies of marine and (3) continent, organic black shale of terrestrial facies [22,23]. Lacustrine organic black shale is mainly distributed in Mesozoic and Cenozoic of lacustrine basins in China such as Cretaceous of Songliao Basin, Paleogene of Bohai Bay Basin, Triassic of Ordos Basin, Triassic and Jurassic of Sichuan Basin, Jurassic of Junggar basin, Jurassic of Turpan Hami basin, Triassic and Jurassic of Tarim Basin and Cenozoic of Qaidam Basin [24–28]. In China, the depth of lacustrine organic black shale is between 500–6000 m [29], and its organic carbon content is between 2–3%, and the highest is between 7–8% [30,31]. Taking Yanchang Formation of Triassic in Ordos Basin as an example, the development of China's Triassic lacustrine rich-organic black shale has discussed Chang 7 and Chang 9 Member of Yanchang Formation of Upper Triassic as the best developed in Ordos Basin, and these are mainly distributed in the central and southern margin of the basin [32].

With the continuous progress of unconventional oil and gas exploration technology, shale oil has gradually become the focus of the oil and gas industry [33,34]. In America, large-scale shale oil has been found, such as Bakken formation of Williston Basin and EagleFord formation of Western Gulf Basin, and commercial exploitation has been carried out [35]. In China, shale oil resources have also been found in Chang 7 Member of Ordos Basin [36], Hetaoyuan Formation of Biyang Depression and Sha 4 Member of Jiyang Depression [37,38].

As the largest oil and gas production basin in China, the Ordos Basin has become one of the most important sites of shale oil exploration and production. The large-scale exploration and development of shale oil in Chang 7 Member of Ordos Basin began in 2011. The proved oil geological reserves in Chang 7_2 Submember were 1.006×10^8 t in 2014, and the proved reserves in Chang 7_1 and Chang 7_2 Submembers in 2019 were 3.589×10^8 t. However, there is no great breakthrough in the exploration of Chang 7_3 Submember [31,32].

The Late Triassic Yanchang formation is a set of fluvial-lacustrine strata deposited after the development and stable lacustrine conditions in the Ordos Basin. The basin was the largest in size during the Chang 7 sedimentary period. The rich-organic black shale and dark mudstone of Chang 7 almost covered most of the basin, providing sufficient oil for the reservoirs of Yanchang formation and even Yan'an formation [39–44]. Nevertheless, there are still several questions, such as how such high-quality shale was formed? What was the paleoenvironment during the deposition of Chang 7 shale? What is the enrichment mechanism of OM in Chang 7 shale? There are still three main disputes. Therefore, this study aims to reconstruct climate change in the Late Triassic and to clarify the enrichment mechanism of Triassic lacustrine OM of continent.

2. Geoglogical Setting

The Ordos Basin, located in North-Central China, is a typical multi-cycle superimposed basin [45–47], is rectangular as a whole and is surrounded by the Luliang Mountains in the east, Helan Mountain in the west, Yinshan Mountain in the north and Qinling Mountain in the south [48–51]. The Ordos Basin, the second largest sedimentary basin in China, spans five provinces and covers a huge area of 37×10^4 km^2 [49,52–54]. As the second largest sedimentary basin in inland China, Ordos Basin is rich in oil and gas resources, with a total output of more than 7600×10^4 t in 2020, now it has become the largest oil and gas production area in China [55]. The study area is located in the southeast of Ordos Basin (Figure 1a,b).
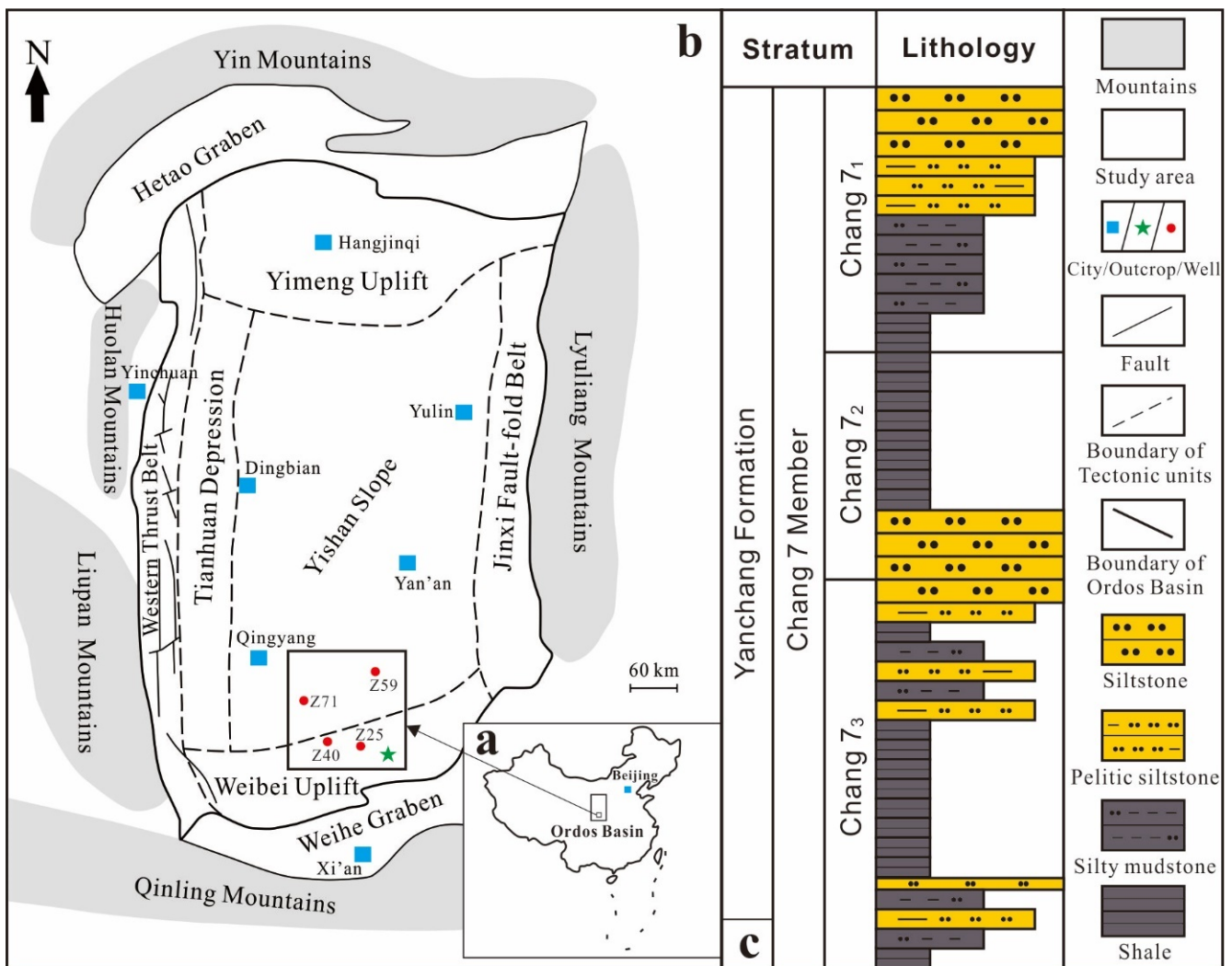
Figure 1. Location map of the area and lithology column of the sampling well. (**a**) Location of the Ordos Basin in China; (**b**) outline and sampling location of this study in Ordos Basin; (**c**) stratigraphic scheme and lithology of the Chang 7 Member in Ordos Basin.

The internal structure of Ordos Basin is very asymmetric. The western edge of the basin is steep and the eastern edge is gentle, and the northwest is high and the southeast is low [56–58]. It can be divided into six primary structural units: the Western Thrust Belt, the western Tianhuan Depression, the central Yishan Slope, the eastern Jinxi Fault-fold Belt, the southern Weibei Uplift and the northern Yimeng Uplift [35,55,59].

At the period of Middle and Late Triassic, the Ordos Basin entered the development stage of inland lake basin under the influence of the Indosinian movement. There were multiple sets of source-reservoir-cap rocks combination condition in the longitudinal direction. The Yanchang formation completely recorded the whole process of Lake Basin from formation and development to shrinkage [59,60]. The lake facies with thickness of 400~800 m was formed, which interbedded with fluvial facies and delta facies. In fact, during the Chang 7 sedimentary period, the lake transgression scale in the basin reached its largest, leading to the emergence of deep lacustrine facies deposition and the development of thick high-quality shale [31,61].

According to the lithologic characteristics, Chang 7 Member can be divided into three sections vertically. From top to bottom: Chang 7_1, Chang 7_2 and Chang 7_3 [44,62]. At the period of Chang 7 sedimentary, the water depth reached its deepest point. The shales deposited during this period is the best quality in the Triassic strata, which can provide

a good hydrocarbon generation basis for the Yanchang Formation [58]. Following the deposition of Chang 7_1 and Chang 7_2, the water depth reduced gradually, and the sediment was mainly deep lacustrine facies deposition, which was interbedded with siltstone and mudstone, and thin-layer source rocks were developed in some areas (Figure 1c).

3. Samples and Methods

3.1. Samples

TOC, major and trace elements were determined in 12 shale samples from Chang 7 outcrop in the east of Weibei uplift, Ordos Basin. Moreover, four samples were collected for biomarker identification, which were from four well core of Chang 7 shale in the southern margin of Ordos Basin. Twelve shale samples of Chang 7 outcrop are used for X-ray diffraction (XRD) analysis. There are six samples (No. H3, H9, H12, Z71, Z59, Z40) used for thin section observation and Scanning Electron Microscopy-Energy Dispersive Spectrometer (SEM-EDS) analysis.

3.2. Experimental Methods

TOC measurement was performed using the Leco CS-200 carbon and sulfur analyzer. Grind the sample to a particle size of less than 0.2 mm. After removing inorganic carbon (>10 g) from the sample with dilute hydrochloric acid, the sample was burned under high-temperature oxygen flows to convert TOC to CO_2. Then, the TOC in the sample was determined by an flame ionization detector (FID).

The major elements, such as SiO_2, TiO_2, Al_2O_3, CaO, Fe_2O_3, K_2O and MgO, were measured by a wavelength dispersive X-ray fluorescence (XRF) spectrometer (ZSX PrimusII). The XRF analysis follows "Verification regulation for wavelength dispersive X-Ray fluorescence spectrometer" (the national measurement standard of the People's Republic of China JJG 016-2004). There are 60 g powder of each sample used for the analysis. The sample was dissolved with anhydrous lithium tetraborate, ammonium nitrate as oxidant, lithium fluoride and a small amount of lithium bromide as cosolvent and release agent, respectively. The ratio of sample to reagent is 1:8. Glass samples were prepared at 1150–1250 °C using a sample melting machine. Ten major elements were obtained for each sample. The contents of six metal ions were determined by conversion. The analytical error of the major elements is less than 1%.

The trace elements, such as Ba, Mn, Sr, Zn, V, Zr, Cr, Rb, Ni, in the samples were directly determined by the external standard method of inductively coupled plasma mass spectrometry (Perkin Elmer NexION 350X). There was 60 g powder of each sample used for the analysis. First, the sample was dissolved in hydrofluoric acid and nitric acid in a closed vessel. The hydrofluoric acid was then removed by evaporation using a hot plate. Then, the sample was dissolved in nitric acid under sealed conditions for determination. A total of 40 trace elements were detected from the samples. The trace element data were compared with the data from the international standard substance of United States Geological Survey. The analytical error of the trace elements was less than 5%.

The more samples there are, the more obvious the statistical significance is and the more geological significance can be reflected. To establish the relationship between TOC and the different major/trace elements, statistical analysis was performed in Chang 7 Member of the study area. Due to the low number of samples of Chang 7_2 Member, the correlation coefficient (R^2) data refers only to Chang 7_3 Member.

After the pretreatment of source rock samples, the source rock extract was obtained by a Soxhlet extractor method. There are 100 g powder of each sample used for the analysis. Gas chromatography-mass spectrometer (GC-MS) analysis was obtained by Agilent 7890A/7000 GC/MS system. Firstly, the source rock extract and crude oil were dilutedthrough *n*-hexane and centrifuged for 5 minutes. After that, supernatant was taken and separated by silica a gel/alumina (3:2) chromatography column. Then, 25 mL of *n*-hexane was slowly dripped into the column to obtain saturated hydrocarbons. Next, a GC-MS system was used to analyze the separated saturated hydrocarbon components.

To analyze the saturated fractions, set the initial GC oven temperature to 50 °C for 1 min, whereupon the temperature will rise 20 °C every minute to 120 °C, and then the temperature will rise 3 °C every minute to 310 °C and stay at this temperature for 30 min. Calculate the peak area, the results of geochemical parameters of the samples are obtained.

The XRD analysis is mainly based on "X-ray diffraction analysis method of clay minerals and common non clay minerals in sedimentary rocks" (the oil and gas industry standard of the People's Republic of China SY/T 5163–2010), and the whole rock XRD analysis of shale samples is carried out by using X-ray diffractometer (Panalytical X'Pert PRO). There was 50 g powder of each sample used for the analysis. The 2-theta range of the XRD analysis is 5–45°. The test was completed by the Nuclear Industry Geological Analysis and Test Research Center of China.

The thin section observation was completed mainly according to the national standard of the People's Republic of China GB/T 35206-2017, and the thin sections of shale were observed by a polarizing microscope (Lecia DM4500P/DFC450C). This work was carried out by the modern analysis and testing center of Xi'an Shiyou University. The SEM-EDS analysis follows the national standard of the People's Republic of China GB/T 17,359–2012 and uses a field emission scanning electron microscope (JEOL-7600F) and an energy spectrometer (X-Max50) to analyze shale samples. There was an 80-g block of each sample used for the analysis. The coating type used was gold, the range of working distance was 8.0–16.0 mm, the range of offset was 2.5–3.0 mm. The test was completed by the Experimental Test Center of Xi'an Geological Survey Center of China Geological Survey.

4. Results

4.1. Total Organic Carbon Contents

The TOC of 12 samples in Chang 7_2 and Chang 7_3 shale is distributed, ranging from 4.84–6.03%, with an average value of 5.68%. The TOC of all samples are more than 4%, and the TOC of most samples is between 5–6% (Table 1), which could imply high oil-generation potential [63].

Table 1. The measured values of TOC and major and trace elements in Chang 7 outcrop shale.

No.	Stratum	TOC (%)	Ba/Al	P/Ti	C	V/Cr	V/(V + Ni)	Sr/Ba	Fe/Mn	CIA	SiO$_2$ (%)	TiO$_2$ (%)	Fe + K (%)	Si/(Si + Al + Fe)	Fe/Ti	U/Th	Eu (ppm)
H1	Chang7$_2$	5.85	72.85	0.54	0.71	3.65	0.90	0.35	127.30	70.19	36.42	0.43	9.47	0.55	37.60	4.90	1.23
H2	Chang7$_2$	5.96	72.86	0.51	0.63	3.52	0.89	0.31	190.13	76.40	40.61	0.32	9.23	0.57	30.71	1.28	1.19
H3	Chang7$_2$	5.93	81.88	0.91	0.50	3.91	0.89	0.50	142.77	69.19	46.90	0.46	8.17	0.64	30.75	5.68	1.29
H4	Chang7$_3$	5.47	86.70	0.56	0.38	2.76	0.84	0.30	38.19	72.34	44.44	0.51	7.72	0.61	18.39	1.35	1.28
H5	Chang7$_3$	5.22	86.01	0.53	0.39	2.35	0.83	0.30	35.48	70.18	46.51	0.53	7.07	0.64	16.75	1.80	1.20
H6	Chang7$_3$	4.84	78.55	0.31	0.36	2.18	0.82	0.27	42.98	75.70	48.17	0.63	7.65	0.63	14.11	0.91	1.39
H7	Chang7$_3$	5.20	92.78	0.67	0.48	4.55	0.90	0.33	78.62	68.81	45.36	0.40	8.46	0.62	28.66	4.32	1.16
H8	Chang7$_3$	5.85	111.51	0.66	0.35	4.20	0.91	0.57	42.47	69.01	43.58	0.36	8.59	0.60	25.61	5.13	1.42
H9	Chang7$_3$	6.03	114.66	0.86	0.28	4.49	0.89	0.50	28.81	71.28	46.09	0.40	7.54	0.63	23.87	4.13	1.84
H10	Chang7$_3$	6.01	53.14	0.60	0.41	3.18	0.85	0.29	69.78	72.99	45.73	0.30	7.86	0.18	27.99	3.63	1.04
H11	Chang7$_3$	5.99	117.05	0.77	0.35	5.27	0.92	0.50	114.25	72.89	43.33	0.32	7.43	0.61	31.38	6.39	1.42
H12	Chang7$_3$	5.79	118.26	0.62	0.39	4.63	0.92	0.41	96.59	73.26	44.26	0.41	8.70	0.61	33.04	3.70	1.46

Note: C value = (C$_O$ + Fe + Mn + Cr + Ni + V)/(Ca + Mg + Sr + Ba + K + Na); Chemical index of alteration (CIA) = Al$_2$O$_3$/(Al$_2$O$_3$ + CaO + Na$_2$O + K$_2$O) × 100. The original data of major and trace elements are respectively shown in Tables S1 and S2 of Supplementary Materials.

4.2. Major and Trace Element Geochemistry

Concentrations and ratios of trace elements could be useful parameters for the reconstruction of sedimentary paleoenvironment [64–66]. The major elements of the studied samples have SiO$_2$ and TiO$_2$, and the ratio of the major element oxides CIA is also included (Table 1). The trace elements of the studied samples are mostly presented in the form of ratios, which are mainly related to these trace elements (Ba, Al, P, Fe, Mn, Ti, Sr, V, Cr, Ni, U, Th) (Table 1).

The Ba/Al ratio in Chang 7 shale is between 53.14–118.26, with an average value of 90.52. The P/Ti ratio is between 0.31–0.91, and the average value is 0.63. The V/Cr ratio is between 2.18–5.27, and the average value is 3.72. The V/(V + Ni) ratio is between 0.82–0.92, and the average value is 0.88. The Sr/Ba ratio is between 0.27–0.57, and the average value is 0.39. The Fe/Mn ratio is between 28.81–190.13, and the average value is 83.95. The ratio of Si/(Si + Al + Fe) is between 0.18–0.64, and the average value is 0.57. The Fe/Ti ratio is

between 14.11–37.60, with an average of 26.57. The U/Th ratio is between 0.91–6.39, with an average of 3.52 (Table 1).

4.3. Molecular Geochemical Characteristics

4.3.1. *n*-alkanes and Isoprenoids

The carbon number of *n*-alkanes in Chang 7_3 shale is between C_{13}–C_{33}, and the main peak is between $C_{16/17}$–C_{22}, which has the advantage of low carbon number and presents the characteristics of front, and Pr/Ph are less than 1 (Figure 2a,b and Table 2).
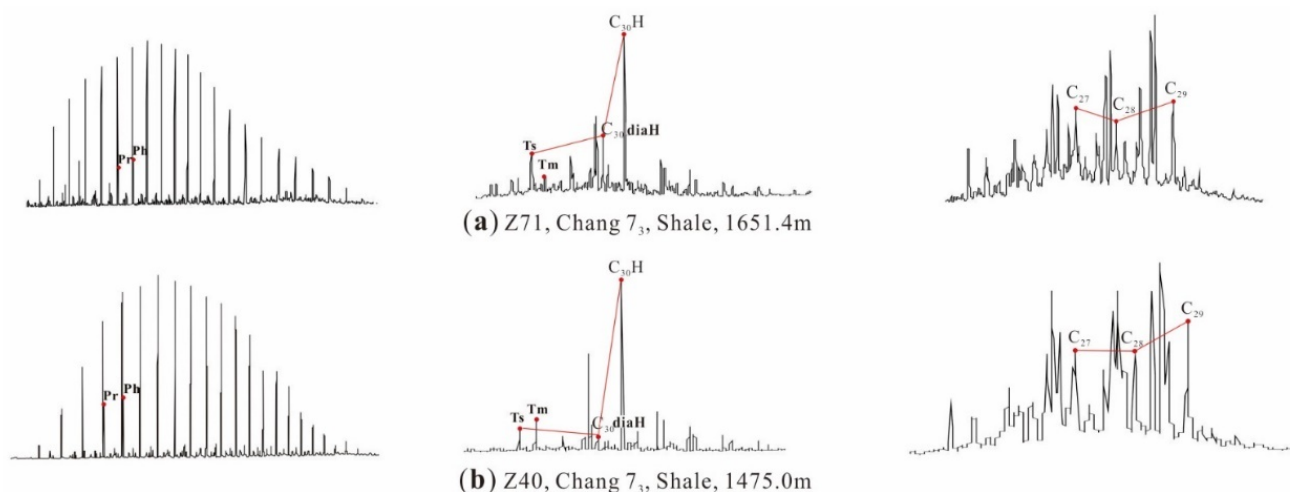

Figure 2. Mass spectra of m/z191 and m/z217 and saturated hydrocarbon chromatography from Chang 7_3 shale of typical well: (**a**) the sample at 1651.4 m from Well Z71; (**b**) the sample at 1475.0 m from Well Z40).

Table 2. The geochemical indexes extracting from well samples of Chang 7_3 shale.

Well	Stratum	Depth/m	Lithology	Pr/Ph	C_{27}/C_{29}	Ts/Tm	$C_{30}H/C_{30}diaH$
Z59	Chang 7_3	1263.2	Shale	0.62	0.65	1.44	8.15
Z71	Chang 7_3	1651.4	Shale	0.75	0.82	1.15	5.77
Z25	Chang 7_3	1070.6	Shale	0.93	0.69	0.36	12.31
Z40	Chang 7_3	1475.0	Shale	0.97	0.61	0.62	10.16

4.3.2. Steranes and Terpanes

The main peak of Chang 7_3 shale is $C_{30}H(17\alpha(H)$-C_{30}hopane), and the abundance of $C_{30}diaH(17\alpha(H)$-C_{30}diahopane) is the least relatively; however, the relative abundance of norhopane (Ts and Tm) is different in different samples. In fact, the Ts value of sample in the north of the area (such as well Z59 and well Z71) is significantly greater than the Tm value, and Ts/Tm > 1, $C_{30}H/C_{30}diaH$ < 10 (Figure 2a). Meanwhile, the one in the south of the area (such as well Z25 and well Z40) is exactly the opposite. The distribution characteristics of regular steranes of $\alpha\alpha\alpha$-20R are relatively uniform, characterized by $C_{29} > C_{27} > C_{28}$, and C_{27}/C_{29} values are less than 1 (Figure 2a,b).

4.4. Mineral Constituent of Shale

In order to make clear the mineral constituent of Chang 7_2 and Chang 7_3 shale, the whole rock XRD analysis is mainly performed on outcrop shale. The minerals were detected by XRD, including quart, feldspar, dolomite, calcite, pyrite, illite/smectite formation, illite, kaolinite, and chlorite (Table 3) illite/smectite formation, illite, kaolinite, and chlorite belongs to clay minerals. The average contents of dolomite, calcite, kaolinite, and chlorite are all less than 5% (Table 3). The content of illite/smectite formation is between 18.4–27.3%, and the average value is 23.2%. The content of illite is between 10.6–18.2%, with an average

value of 13.9%. The content of pyrite is between 14.2–19.3%, and the average value is 16.7%. The content of quartz is between 23.0–34.3%, with an average value of 29.0%. The content of feldspar is between 9.6–20.4%, and the average value is 15.1% (Table 3).

Table 3. The XRD analysis of the minerals from Chang 7 outcrop shale.

No.	Stratum	Quartz (%)	Feldspar (%)	Dolomite (%)	Calcite (%)	Pyrite (%)	Illite/Smectite Formation (%)	Illite (%)	Kaolinite (%)	Chlorite (%)
H1	Chang 7_2	30.3	12.0	3.2		15.3	25.4	12.4		1.4
H2	Chang 7_2	30.1	14.8		1.4	14.2	24.9	14.6		
H3	Chang 7_2	31.5	11.3	1.6		16.4	22.7	15.2		1.3
H4	Chang 7_3	32.3	18.3		0.4	17.2	19.5	12.3		
H5	Chang 7_3	25.8	16.7	3.7		16.9	23.6	11.7		1.6
H6	Chang 7_3	33.2	20.4		1.6	15.8	18.4	10.6		
H7	Chang 7_3	27.4	16.6	0.5	0.3	18.4	23.5	11.5	0.8	1.0
H8	Chang 7_3	31.1	17.3			14.2	22.8	14.3	0.3	
H9	Chang 7_3	24.2	9.6		1.8	18.7	27.3	17.7		0.7
H10	Chang 7_3	23.0	12.7			19.3	25.8	18.2	1.0	
H11	Chang 7_3	24.9	16.2			18.1	24.5	16.3		
H12	Chang 7_3	34.3	15.0	2.5		16.0	20.1	12.1		
	Average	29.0	15.1	2.3	1.1	16.7	23.2	13.9	0.7	1.2

4.5. Volcanic Tuff and Hydrothermal Mineral in Shale

Under a polarizing microscope, the outcrop shale thin section of Chang 7 was observed [67,68]. Ash tuff was found in sample H3, and pyrite was sporadically distributed (Figure 3a). Crystal debris tuff appeared in sample H9, in which the crystal debris was mainly albite and potash feldspar. The surface of albite was relatively clean, and the surface alteration of potash feldspar was obvious (Figure 3b). In sample H12, vitric-crystal debris tuff was observed, vitric debris was mostly striped or irregular, crystal debris was mainly albite, and there was pyrite distribution (Figure 3c). The appearance of these tuffs indicates that the Chang 7 deposit was affected by volcanic activity in the study area.

Through SEM-EDS analysis, subglobular marcasite and ortho-octahedral pyrite were found in the Chang 7_3 shale SEM image of well Z71 (Figure 3d). Framboidal pyrite appeared in the Chang 7_3 shale SEM image of Well Z59 (Figure 3e,f). Petaloid anhydrite could be seen in the Chang 7_3 shale SEM image of Well Z40 (Figure 3g,h). These characteristic minerals of SEM-EDS identification are considered as typical minerals reflecting low-temperature hydrothermal activities of the depositional period.
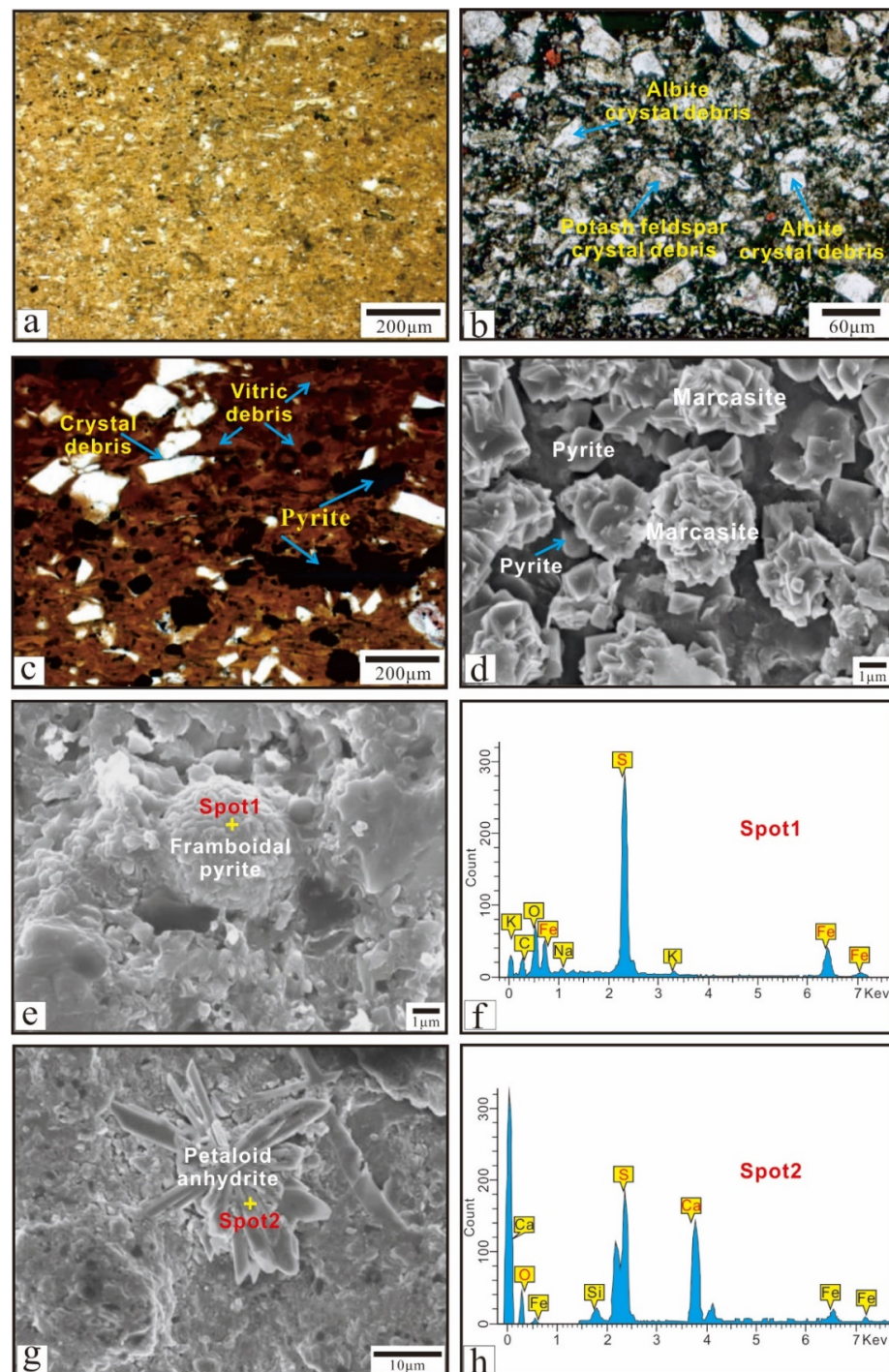
Figure 3. The thin section images of volcanic tuff and SEM images and EDS data from Chang 7 shale: (**a**) the thin section image of ash tuff under plane polarized light (PPL) in outcrop sample H3 (Chang 7_2); (**b**) the thin section image of crystal debris tuff under cross-polarized light (XPL) in outcrop sample H9 (Chang 7_3); (**c**) the thin section image of vitric-crystal debris tuff under plane polarized light (PPL) in outcrop sample H12 (Chang 7_3); (**d**) the SEM image showing subglobular marcasite and ortho-octahedral pyrite of Well Z71 (Chang 7_3, 1651.4 m); (**e**) the SEM image showing framboidal pyrite of Well Z59 (Chang 7_3, 1263.2 m); (**f**) The EDS data of pyrite of Well Z59 (Chang 7_3, 1263.2 m); (**g**) the SEM image showing petaloid anhydrite of Well Z40 (Chang 7_3, 1475.0 m); (**h**) the EDS data of anhydrite of Well Z40 (Chang 7_3, 1475.0 m).

5. Discussion

5.1. Sedimentary Environment and Its Impact on OM Enrichment

5.1.1. Biological Productivity and Its Impact on OM Enrichment

Biological productivity plays an important role in the enrichment of OM [7,43,69,70]. It is generally believed that there is a positive correlation between biological productivity and shale OM content [71,72]. As a necessary nutrient element for biology, P is usually used to judge biological productivity after Ti correction, P/Ti > 0.79 could be indicators of high productivity, 0.34 < P/Ti < 0.79 represents medium productivity and P/Ti < 0.34 represents low productivity [66]. The Ba contained in organism will form one of the elemental components of barite after biological death, resulting in relative aggregation of Ba, so that the paleoproductivity intensity can also be roughly judged by Ba/Al [65,73,74].

The P/Ti distribution range of Chang-7 shale is between 0.31–0.91, with an average value of 0.63, and the Ba/Al distribution range is between 53.14–118.26, with an average value of 90.52 (Table 2). Moreover, those indices indicate that Chang 7 shale has medium-high biological productivity.

It can be found that there is hardly any correlation between TOC and Ba/Al (Figure 4a) and a positive correlation between TOC and P/Ti (Figure 4b) with the cross-plot of TOC and biological productivity index in Chang 7 shale.
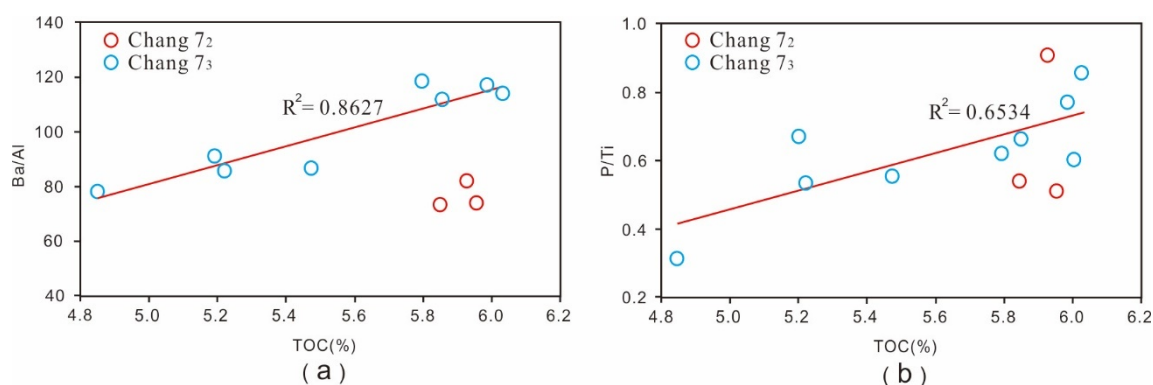

Figure 4. The cross-plot of biological productivity indicators and TOC: (**a**) Relationship between Ba/Al and TOC; (**b**) Relationship between P/Ti and TOC.

It can be found that there is a strong positive correlation between TOC and biological productivity index of Chang 7_3 shale, indicating that high biological productivity is the premise of OM enrichment (Figure 4).

5.1.2. Biomarker Assemblages and Depositional Environments

The distribution of *n*-alkanes and isoprenoids can provide information on the origin and sedimentary environment of OM, which is of great significance to oil source and oil and gas exploration [60,75,76]. Generally, the carbon number distribution range of *n*-alkanes in shale formed with aquatic algae is less than C_{20}, and the *n*-alkane distribution curve is the frontal peak type, reflecting a deep water sedimentary environment. The carbon number distribution of *n*-alkanes in the hydrocarbon source rocks formed with higher plants on land and the main peak is relatively backward, showing shallow water sedimentary environment [44,77]. The shale sample of Chang 7 is characterized by the frontal peak type curve of *n*-alkane distribution, indicating that its parent material is aquatic algae. It has also been reported that low molecular weight n-alkanes may also indicate bacterial modification under some conditions [78].

Steranes and terpanes are the most common biomarkers and have good indicative significance for maturity, sedimentary environment and oil source correlation [79,80]. The relative contents of Pr and Ph are related to the redox environment during OM deposition. Pr/Ph < 1 reflects the weak reducing sedimentary environment, Pr/Ph between

1.0–2.0 reflects the weak reduction weak oxidation mixed sedimentary environment and Pr/Ph > 2 reflects the partial oxidizing sedimentary environment [81–83]. The Pr/Ph of Chang 7 shale samples is less than 1, indicating that the environment of Chang 7 in the area was reductive during the depositional period.

The values of Ts/Tm and $C_{30}H/C_{30}diaH$ are related to the maturity of OM. With the increase of burial depth, the values of Ts/Tm and $C_{30}H/C_{30}diaH$ will usually decrease [80,84]. When there are the same maturity conditions, the ratio also reflects the organic facies of source rocks, which is closely related to the type of source rocks and clay catalysis. The sedimentary environment with high terrigenous clay content (Table 3) and sub-oxidation are more conducive to the formation of Ts and rearranged sterane (such as $C_{30}diaH$) [85,86]. The northern part of the area is close to the middle of the lake basin, with deep water environment and relatively high reducing and a low content of terrigenous clay. However, the Ts and $C_{30}diaH$ of sample are higher than those at the southern part of the area at the edge of the lake basin. This indicates that the reason for the difference between the north part and the south one has nothing to do with clay catalysis and oxygenation reducing but has a greater relationship with maturity.

The biomarker assemblages are different in shale from different parent material. In humic shale, the relative content of C_{29} sterane is higher and that of C_{27} sterane is lower. On the contrary, better quality shale with sapropelic parent material shows the characteristics that the relative content of C_{27} sterane is greater than that of C_{29} sterane [87,88]. The high C_{29} sterane of sample reflects the input of some proportion of terrigenous higher plants in the sedimentary period of Chang 7 shale, which is consistent with the sedimentary background that the area is located at the edge of the basin and is subject to terrigenous input from the Qinling Mountains.

5.1.3. Climate Conditions

Through the restoration of ancient latitude and the analysis of a large number of sporopollen fossils, previous researchers confirmed that the southern Ordos basin should be under the tropical-subtropical warm and humid paleoclimate during the Chang 7 depositional period [89–91].

The composition, distribution and relative content of elements in lake sediments can reflect the characteristics of paleoclimatic conditions accurately. In warm and humid climate, elements such as Fe, Mn, Cr, V, Ni and Co are more vulnerable to weathering and denudation, thus transporting to the lake [92,93]. On the other hand, in arid and hot climate, a large number of elements will precipitate, such as Ca, Mg, K, Na, Sr, Ba, etc., due to the continuous evaporation of water and the enhancement of water alkalinity [94,95]. Paleoclimatic conditions can be reconstructed by using the ratio (C value) of these two kinds of elements [96,97]. According to the C value of Table 1, climate can be divided into arid, semi-arid, semi-humid and semi-arid, semi-humid and humid, and they correspond to C < 0.2, 0.2 < C < 0.4, 0.4 < C < 0.6, 0.6 < C < 0.8 and C > 0.8, respectively. In addition, paleoclimate can affect the weathering intensity and rock composition of parent rock. Chemical Index of Alteration (CIA) is an effective indicator parameter of paleoclimate, and its calculation equation is shown in Table 1 [95]. According to the CIA values, climate can be divided into cold, dry, warm and humid, and the correspond to 40–50, 50–65, 65–85 and 85–100, respectively.

The C value of Chang 7 shale is between 0.28–0.71, with an average value of 0.44, while the CIA value is between 68.81–76.40, with an average value of 71.85 (Table 1). This indicates that the sedimentary period of Chang 7 is a warm and humid climate. On the cross-plot of paleoclimate indicators (C value and CIA) and TOC (Figure 5), it is difficult to find a correlation between them, indicating that paleoclimate conditions are not the main controlling factor affecting the enrichment of OM in Chang 7 shale.
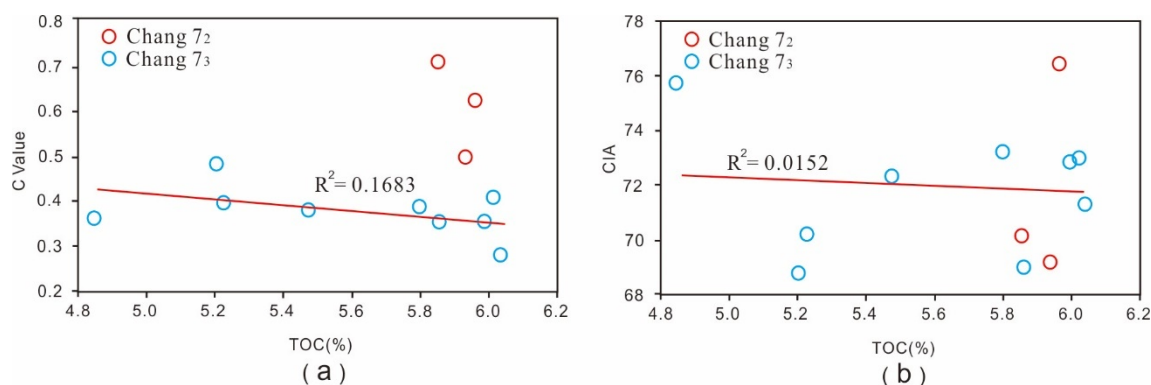
Figure 5. The cross-plot of paleoclimate indicators and TOC: (**a**) relationship between C and TOC; (**b**) relationship between CIA and TOC.

5.1.4. Paleowater Conditions

Siderophile elements such as V, Ni, U, Mn and Cr are redox-sensitive elements. They have different chemical behaviors in different redox environments and can be used as the discrimination index of a redox environment. $V/(V + Ni) > 0.77$ indicates a reductive environment, and $V/(V + Ni) < 0.6$ indicates an oxygen-enriched environment [98,99]. In addition, V/Cr can also be used as an indicator of redox environment. $V/Cr < 2$ indicates oxygen enrichment conditions, $2 < V/Cr < 4.25$ indicates transition conditions and $V/Cr > 4.25$ indicates anoxic environment [100,101]. The occurrence forms of Sr and Ba are bicarbonate in the lake. When the salinity of a lake increases, Ba precipitates before Sr, which is why the value of Sr/Ba can reflect the change of salinity. Generally, $Sr/Ba < 1$ represents a fresh water environment and $Sr/Ba > 1$ represents a salt water environment [102,103]. The Fe/Mn ratio can be used to indicate the water depth. The greater the ratio, the shallower the water depth [104,105].

The $V/(V + Ni)$ value of Chang 7 shale is between 0.82–0.92, with an average value of 0.88. The V/Cr is between 2.18–5.27, with an average value of 3.72; Sr/Ba is between 0.27–0.57, with an average of 0.39; the Fe/Mn is between 28.81–190.13, with an average of 83.95 (Table 1). The results show that the depositional environment of Chang 7 shale is reductive freshwater.

On the cross-plot of redox conditions, salinity, water depth and TOC, it can be found that there is a weak positive correlation between redox conditions (V/Cr and V/(V + Ni)) and TOC (Figure 6a,b). To some extent, this indicates that a reducing environment is beneficial to the preservation of OM. It can also be seen from the relationship between water depth (Fe/Mn) and TOC (Figure 6c). In addition, there is a weak positive correlation between salinity (Sr/Ba) and TOC (Figure 6d), indicating that a fresh water environment may be conducive to the enrichment of OM in the background of overall fresh water.

5.1.5. Terrestrial Inputs and Hydrodynamic Conditions

As stable terrestrial major elements, SiO_2, TiO_2, Al_2O_3, K_2O and Na_2O are used to indicate terrestrial inputs distinctly [106,107]. In addition, Fe + K, which is stable as a kind of terrestrial trace elements index, is also a common index for characterizing the input of terrigenous debris. The higher its value, the stronger the terrestrial inputs [108,109]. $Si/(Si + Al + Fe)$ can provide information related to the distance from the provenance area. This value decreases with the increase of the distance from the provenance area. A higher ratio means that it is closer to the provenance area and vice versa [110].

The content of $TiO_2 + Al_2O_3 + SiO_2$ is between 19.56–66.72 ppm in Chang 7 shale, with an average of 54.70 ppm. The content of Fe + K is between 7.07–9.47 ppm, with an average of 8.16 ppm. The content of $Si/(Si + Al + Fe)$ is between 0.18–0.64, with an average value of 0.57 (Table 1). The results indicate that there are some terrestrial inputs of Chang 7 shale, and the area is not far from the provenance area.
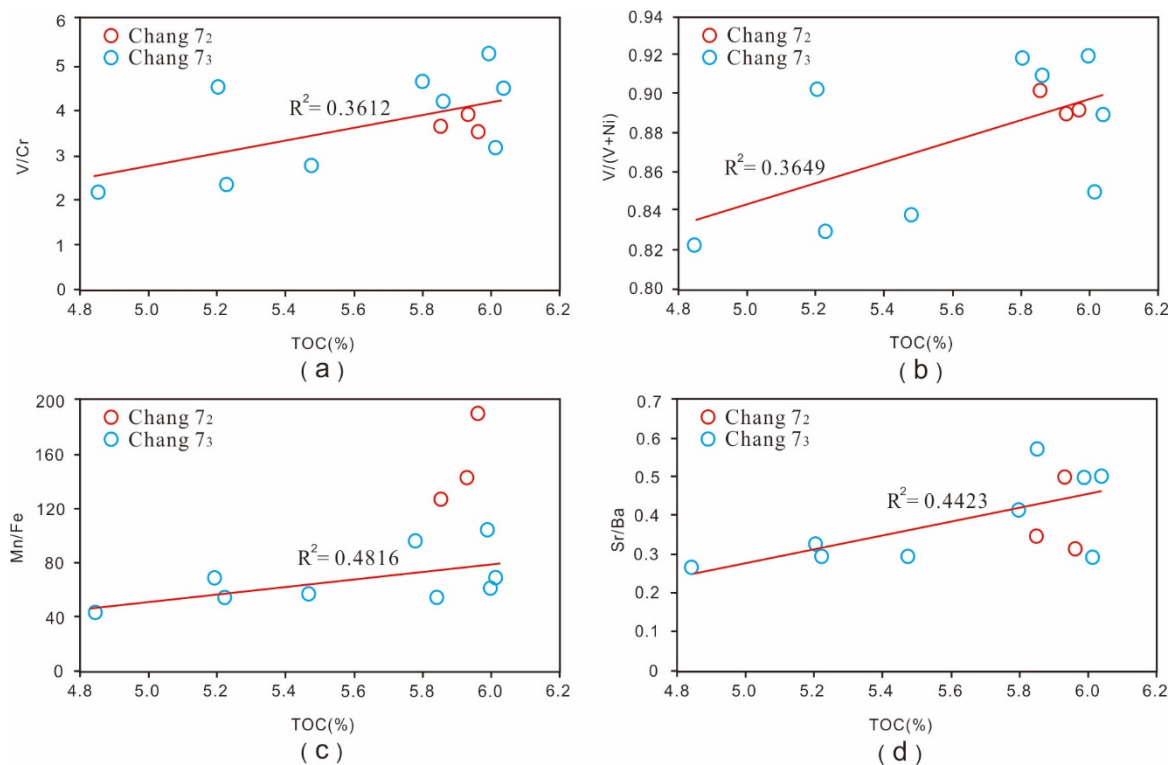
Figure 6. The cross-plot of paleowater conditions indicators and TOC: (**a**) relationship between V/Cr and TOC; (**b**) relationship between V/(V + Ni) and TOC; (**c**) relationship between Mn/Fe and TOC; (**d**) relationship between Sr/Ba and TOC.

There is an obvious negative correlation between terrestrial inputs indicators (TiO$_2$ and SiO$_2$) and TOC (Figure 7), indicating that the parent material of OM is mainly aquatic organisms. Moreover, terrestrial inputs will dilute the OM and is not conducive to the preservation of OM.
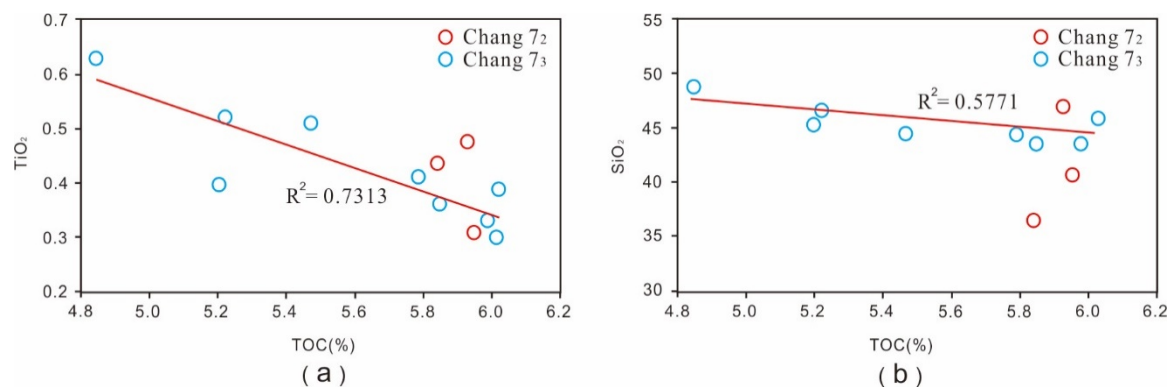
Figure 7. The cross-plot of terrestrial inputs indicators and TOC: (**a**) relationship between TiO$_2$ and TOC; (**b**) relationship between SiO$_2$ and TOC.

5.1.6. Volcanism and Hydrothermal Activity

Volcanism and hydrothermal activities at the bottom of lake would bring a lot of heat and nutrient elements, which is conducive to the development of organisms, and then affect the enrichment of OM. The study of volcanism and hydrothermal activities in the sedimentary period of Chang 7 shale is a research hotspot in recent years [111]. Generally, sediments formed by volcanism and hydrothermal activities have abnormal element geochemical characteristics, including obvious Eu anomaly, enrichment of heavy rare earth elements and high Fe/Ti [112–114].

The Eu value of Chang 7 shale is high, between 1.04–1.84 ppm, with an average value of 1.33 ppm; Fe/Ti is between 14.11–37.60, with an average value of 26.57; U/Th is between 0.91–6.39, with an average value of 3.52 (Table 1). In addition, hydrothermal sediments and tuff formed by volcanic ash developed in Chang 7 shale and dense microfossils of thermophilic algae are seen in thin sections under the microscope, indicating that the Chang 7 shale experienced volcanism and hydrothermal activities during the sedimentary period. However, scholars have not found tectonic evidence of volcanic activity around Ordos Basin until the present moment.

At present, there is controversy about the impact of volcanism and hydrothermal activities at the bottom of the lake on the enrichment of OM in Chang 7 shale. Some scholars believe that volcanism and hydrothermal activities have brought rich nutrient elements, promoted the growth of organisms and increased the enrichment of OM in sediments [115]. However, other scholars believe that hydrothermal activities will destroy the inherent OM in sedimentary rocks and adversely affect the development and preservation of OM [116]. During the Indosinian movement, Ordos Basin experienced basement fault activity. Frequent volcanic eruptions and hydrothermal upwelling in deep water in Qinling orogenic belt coincided with the deposition of Yanchang formation. Volcanism and hydrothermal activities at the bottom of the lake had an important impact on Chang 7 shale [111,117–119]. There is a positive correlation between the hydrothermal activity indexes and TOC (Figure 8), indicating that the hydrothermal activity at the bottom of the lake has played a positive role in the enrichment of OM in Chang 7 shale and improved the abundance of lake sedimentary OM.
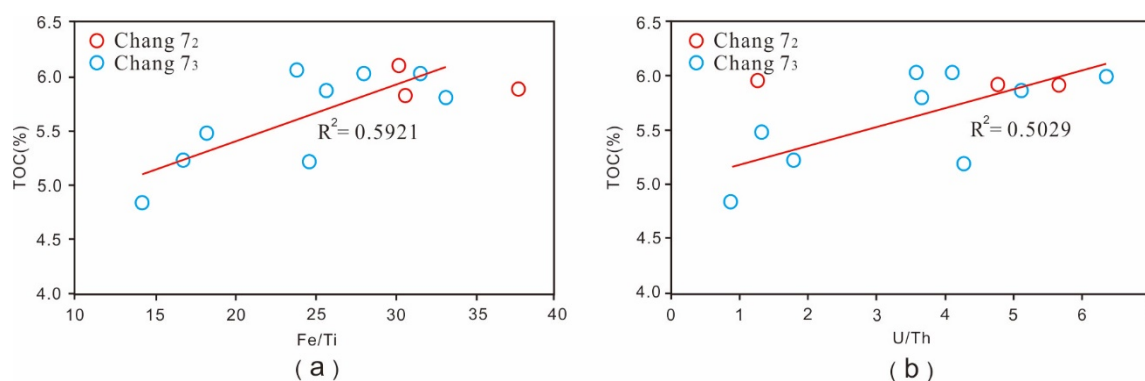

Figure 8. The cross-plot of volcanism and hydrothermal activity indexes and TOC: (**a**) relationship between Fe/Ti and TOC; (**b**) relationship between U/Th and TOC.

The discovery of tuff, XRD data, SEM images and EDS data confirmed that the Chang 7 depositional period in this area was once affected by volcanic and hydrothermal activities at the bottom of the lake from the aspects of petrology and mineralogy, which increased the temperature of Chang 7 deposition. In this study, a series of low-temperature hydrothermal minerals were found in Chang 7 shale: dolomite, calcite, marcasite, pyrite, anhydrite, etc. (Table 3, Figure 3).

Previous researchers have suggested that relatively low temperature hydrothermal fluids can promote the enrichment of organic matter in source rocks, while relatively high temperature hydrothermal fluids may destroy the preservation of organic matter in source rocks [120]. Therefore, the petrological and mineralogical evidence inferred from the above results can also show that volcanism and hydrothermal activities at the bottom of the lake have played a positive role in the enrichment of OM in Chang 7 shale and improved the abundance of lake sedimentary OM in the southern margin of Ordos Basin.

5.2. Enrichment Model of Lacustrine OM

The geochemical data show that the TOC of Chang 7 shale has a strong positive correlation with biological productivity, an obvious negative correlation with terrestrial input, a

weak positive correlation with reducing, salinity and hydrothermal activity intensity and has no inevitable connection with climate conditions and other environmental indicators. In fact, it indicates that high productivity, low consumption and low dilution have created high OM of Chang 7 shale.

Based on the discussion of this study, the enrichment model of Chang 7 shale OM in the southern margin of Ordos Basin is proposed (Figure 9): during the deposition period of Chang 7 shale, the sedimentary environment of Ordos Basin is stable, supporting the large-scale development of deep lacustrine facies. Hydrothermal activities at the bottom of the lake brought a lot of nutrients and promoted the flourish of organisms; in warm and humid climate, evaporation was weak, water salinity was low, salinity stratification interface was deep (according to the discussion of "5.1.4 Paleowater conditions") and the reduction and brackish environment formed in the middle and lower part of the deep water area of the lake basin was conducive to the preservation of OM. In shallow water, OM underwent strong oxidation and decomposition. Terrigenous inputs not only brought terrestrial OM, but also stirred the lake water, inhibited the development of aquatic organisms and increased the oxidation and decomposition extent of OM (according to the discussion of "5.1.5 Terrestrial inputs and hydrodynamic conditions"), which was not conducive to the enrichment and preservation of OM.
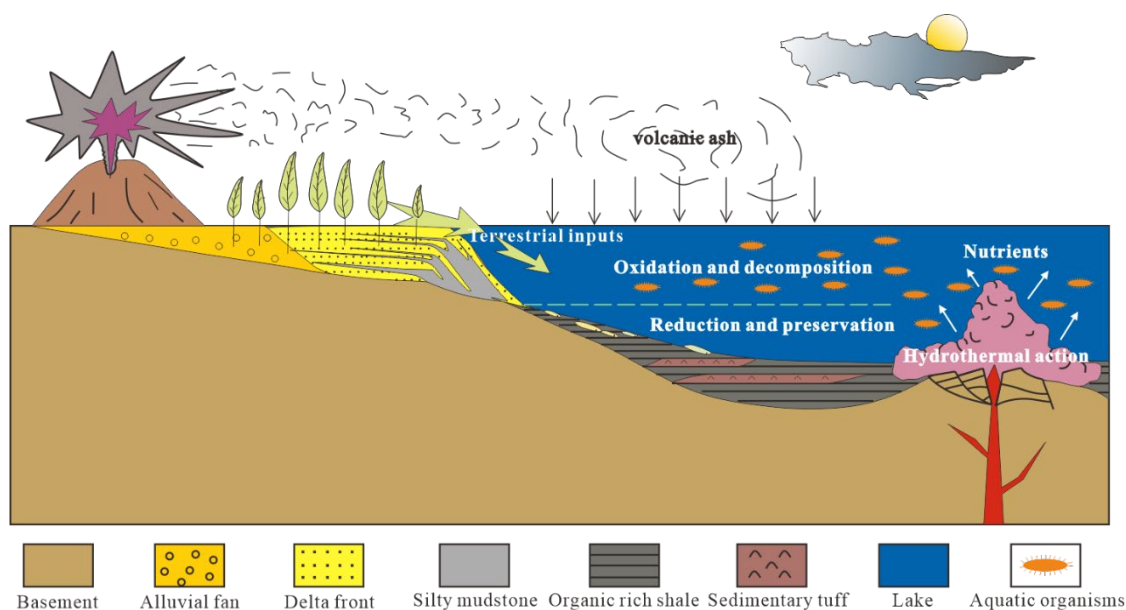

Figure 9. Enrichment model of OM in Chang 7 shale of the southern margin of Ordos Basin.

6. Conclusions

The parent material of Chang 7 shale is mainly algae in the south of Ordos Basin. The sedimentary environment is deep lake, which is reductive and affected by the inputs of terrestrial higher plants.

The climate was warm and humid, the water body was reductive and there was low salinity in the sedimentary period of Chang 7 shale. The area was not far from the provenance area, the water deep changed rapidly, the main origin of OM was algae, but it was also affected by terrestrial OM to a certain extent, and there are very few parts of OM that are terrestrial, and there is also hydrothermal activity at the bottom of the lake. The paleoclimate of Chang 7 shale in the south of Ordos Basin was temperate and subtropical warm and humid or had a humid climate, the topographic slope in the south of the lake basin was steep and the supply source of Qinling Mountain in the South was sufficient.

The hydrothermal activity at the bottom of the lake basin promotes the proliferation of algal organisms and the highly reductive environment is conducive to the preservation of OM. However, terrigenous inputs inhibit the development of aquatic organisms and

increase the oxidation and decomposition extent of OM, which is not conducive to the enrichment and preservation of OM.

References

1. Miall, A.D. Architectural-element analysis: A new method of facies analysis applied to fluvial deposits. *Earth-Sci. Rev.* **1985**, *22*, 261–308. [CrossRef]
2. Miall, A.D. Chapter Two—Sequence Stratigraphy and Geologic Time. *Stratigr. Timescales* **2017**, *2*, 59–83.
3. Lüning, S.; Craig, J.; Loydell, D.K.; Štorch, P.; Fitches, B. Lower Silurian 'hot shales' in North Africa and Arabia: Regional distribution and depositional model. *Earth-Sci. Rev.* **2000**, *49*, 121–200. [CrossRef]
4. Mohamed, W.A.; Aljubouri, Z.A.; Aldobouni, I.A. Depositional environment of the Lower Silurian Akkas hot shales in the Western Desert of Iraq: Results from an organic geochemical study. *Mar. Pet. Geol.* **2015**, *64*, 294–303.
5. Jarvie, D.M.; Hill, R.J.; Ruble, T.E.; Pollastro, R.M. Unconventional shale-gas systems: The Mississippian Barnett Shale of north-central Texas as one model for thermogenic shale-gas assessment. *AAPG Bull.* **2007**, *91*, 475–499. [CrossRef]
6. Potter, C.J. Paleozoic shale gas resources in the Sichuan Basin, China. *AAPG Bull.* **2018**, *102*, 987–1009. [CrossRef]
7. Pedersen, T.F.; Calvert, S.E. Anoxia vs. productivity: What controls the formation of organic-carbon-rich sediments and sedimentary rocks? *AAPG Bull.* **1990**, *74*, 454–466.
8. Sageman, B.B.; Lyons, T.W. Geochemistry of Fine-grained Sediments and Sedimentary Rocks. *Treatise Geochem.* **2003**, *7*, 115–158.
9. Michael, A.A.; Walter, E.D.; Kirsten, L. Organic carbon accumulation and preservation in surface sediments on the Peru margin. *Chem. Geol.* **1998**, *152*, 273–286.
10. Haydon, M.; Olivier, J.; Thierry, A.; Philip, S.; Karl, F.; Virginie, M.; Zsolt, B.; Doris, S. The Cenomanian/Turonian anoxic event at the Bonarelli Level in Italy and Spain: Enhanced productivity and/or better preservation? *Cretac. Res.* **2007**, *28*, 597–612.
11. McArthur, J.M.; Algeo, T.J.; Schootbrugge, B.; Li, Q.; Howarth, R.J. Basinal restriction, black shales, Re-Os dating, and the Early Toarcian (Jurassic) oceanic anoxic event. *Paleoceanography* **2008**, *23*, 1–22. [CrossRef]
12. Demaison, G.J.; Moore, G.T. Anoxic environments and oil source bed genesis. *Org. Geochem.* **1980**, *2*, 9–31. [CrossRef]
13. Hugh, C.J. The early Toarcian (Jurassic) anoxic event; stratigraphic, sedimentary and geochemical evidence. *Am. J. Sci.* **1988**, *288*, 101–151.
14. Röhl, H.J.; Schmid-Röhl, A. Lower Toarcian (Upper Liassic) Black Shales of the Central European Epicontinental Basin: A Sequence Stratigraphic Case Study from the Sw German Posidonia Shale. *Spec. Publ.* **2005**, *82*, 165–189.
15. Słowakiewicz, M.; Tucker, M.E.; Perri, E.; Pancost, R.D. Nearshore euxinia in the photic zone of an ancient sea. *Palaeogeogr. Palaeoclimatol. Palaeoecol.* **2015**, *426*, 242–259. [CrossRef]
16. Algeo, T.J.; Herrmann, A.D. An ancient estuarine_circulation nutrient trap: The Late Pennsylvanian Midcontinent Sea of North America. *Geology* **2018**, *46*, 143–146. [CrossRef]
17. Shi, Y.Z.; Xi, D.P.; Qin, Z.H.; Tong, X.N.; Zhu, X.B.; Yu, Z.Q.; Gu, A.Q.; Song, J.Z.; Hu, J.F.; Wang, X.R.; et al. The biostratigraphy of the 2nd Member of the Nenjiang Formation from the Yuewangcheng section of the eastern Songliao Basin and its response to the lake transgression event. *Geol. Bull. China* **2019**, *38*, 1095–1104.
18. Zheng, R.C.; He, L.; Liang, X.W.; Xu, W.L. Forming conditions of shale gas (oil) plays in the Lower Jurassic Da'anzhai member in the eastern Sichuan Basin. *Nat. Gas Ind.* **2013**, *12*, 30–40.

19. Loucks, R.G.; Reed, R.M.; Ruppel, S.C.; Hammes, U. Spectrum of pore types and networks in mudrocks and a descriptive classification for matrix-related mudrock pores. *AAPG Bull.* **2012**, *96*, 1071–1098. [CrossRef]

20. Wang, X.X.; Hou, J.G.; Li, S.H.; Dou, L.X.; Song, S.H.; Kang, Q.Q.; Wang, D.M. Insight into the nanoscale pore structure of organic-rich shales in the Bakken Formation, USA. *J. Pet. Sci. Eng.* **2020**, *191*, 107182. [CrossRef]

21. Wang, Y.; Liu, L.F.; Cheng, H.F. Gas adsorption characterization of pore structure of organic-rich shale: Insights into contribution of organic matter to shale pore network. *Nat. Resour. Res.* **2021**, *30*, 2377–2395. [CrossRef]

22. Gu, Z.A.; Zheng, R.C.; Wang, L.; Liang, X.W. Characteristics of shale reservoir of Da'anzhai segment in Fuling area, eastern Chongqing. *Lithol. Reserv.* **2014**, *26*, 67–73.

23. Bao, S.J.; Lin, T.; Nie, H.K.; Ren, S.M. Preliminary study of the transitional facies shale gas reservoir characteristics: Taking Permian in the Xiangzhong depression as an example. *Earth Sci. Front.* **2016**, *23*, 44–53.

24. Zhang, W.Z.; Yang, H.; Li, S.P. Hydrocarbon accumulation significance of Chang 9[1] high-quality lacustrine source rocks of Yanchang Formation, Ordos Basin. *Pet. Explor. Dev.* **2008**, *5*, 557–562. [CrossRef]

25. Liu, Z.J.; Meng, Q.T.; Liu, R. Characteristics and genetic types of continental oil shales in China. *J. Palaeogeogr.* **2009**, *11*, 105–114.

26. Zheng, H.J.; Dong, Y.X.; Wang, X.D. The generation and characteristics of source rocks in nanpu oil-rich depression, Bohai Bay Bsain. *Nat. Gas Geosci.* **2007**, *18*, 78–83.

27. Ni, C.; Hao, Y.; Hou, G.F.; Gu, M.F.; Zhang, L.T. Cognition and Significance of Lower Jurassic Daanzhai Organic Muddy Shell Limestone Reservoir in Central Sichuan Basin. *Mar. Orig. Pet. Geol.* **2012**, *17*, 45–56.

28. Zhang, X.B. Study on the origin of the dolostone inthrcalcated in the black shales in middle permian lucaogou formayion eastern part of southern margin of Junggar Basin. *Acta Sedimentol. Sin.* **1993**, *11*, 133–140.

29. Zou, C.N.; Zhao, Q.; Cong, L.Z. Development progress, potential and prospect of shale gas in China. *Nat. Gas Ind.* **2021**, *41*, 1–14.

30. Zhao, Q.; Wang, H.Y.; Yang, S. Potential of continental shale gas accumulation in medium-and small-sized fault basins in eastern China: A case study from the Fuxin Basin. *Nat. Gas Ind.* **2018**, *38*, 26–33.

31. Zou, C.N.; Dong, D.Z.; Wang, S.J. Geological characteristics, formation mechanism and resource potential of shale gas in China. *Pet. Explor. Dev.* **2010**, *37*, 641–653. [CrossRef]

32. Yao, J.L.; Deng, X.Q.; Zhao, Y.D. Characteristics of tight oil in Triassic Yanchang Formation, Ordos Basin. *Pet. Explor. Dev.* **2013**, *40*, 150–158. [CrossRef]

33. Wang, Y.; Cheng, H.F.; Hu, Q.H.; Liu, L.F.; Jia, L.B.; Gao, S.S.; Wang, Y. Pore structure heterogeneity of Wufeng-Longmaxi shale, Sichuan Basin, China: Evidence from gas physisorption and multifractal geometries. *J. Pet. Sci. Eng.* **2022**, *208*, 109313. [CrossRef]

34. Zou, C.N.; Tao, S.Z.; Hou, L.H. Chapter V shale oil and gas. In *Unconventional Oil and Gas Geology*, 2nd ed.; Zou, C.N., Dong, D.Z., Yang, Z., Eds.; Geological Publishing House: Beijing, China, 2013; pp. 130–134.

35. Luo, C.X.; Zhou, W.H. Shale oil development in US and implications. *Sino-Glob. Energy* **2013**, *18*, 33–40.

36. Wang, H.J.; Ma, F.; Tong, X.G. Assessment of global unconventional oil and gas resources. *Pet. Explor. Dev.* **2016**, *43*, 850–862. [CrossRef]

37. Song, Y.; Li, Z.; Jiang, Z.X. Progress and development trend of unconventional oil and gas geological research. *Pet. Explor. Dev.* **2017**, *44*, 638–648. [CrossRef]

38. Jia, C.Z.; Zheng, M.; Zhang, Y.F. Unconventional hydrocarbon resources in China and the prospect of exploration and development. *Pet. Explor. Dev.* **2012**, *39*, 129–136. [CrossRef]

39. Zhang, D.Q.; Zhang, J.Q.; Wang, Y.F. China's unconventional oil and gas exploration and development: Progress and prospects. *Resour. Sci.* **2015**, *37*, 1068–1075.

40. Yang, H.; Niu, X.B.; Xu, L. Exploration potential of shale oil in Chang 7 Member, Upper Triassic Yanchang Formation, Ordos Basin, NW China. *Pet. Explor. Dev.* **2016**, *43*, 511–520. [CrossRef]

41. Lei, Y.; Luo, X.; Wang, X. Characteristics of silty laminae in Zhangjiatan Shale of southeastern Ordos Basin, China: Implications for shale gas formation. *AAPG Bull.* **2015**, *99*, 661–687. [CrossRef]

42. Huang, Z.; Liu, G.; Li, T. Characterization and control of mesopore structural heterogeneity for low thermal maturity shale: A case study of Yanchang Formation Shale, Ordos Basin. *Energy Fuels* **2017**, *31*, 11569–11586. [CrossRef]

43. Zhang, W.; Yang, W.; Xie, Q. Controls on organic matter accumulation in the Triassic Chang 7 lacustrine shale of the Ordos Basin, central China. *Int. J. Coal Geol.* **2017**, *183*, 38–51. [CrossRef]

44. Lu, Z.X.; Chen, S.J.; He, Q.B.; Li, Y.; Zhang, J.Y.; Wu, Q.B. Relationship between methylphenanthrene distribution and organic matter maturity: A case study of Yangchang Formation Chang 7 source rocks, Ordos Basin, China. *Pet. Sci. Technol.* **2018**, *36*, 1718–1724. [CrossRef]

45. Wu, F.L.; Li, W.H.; Li, Y.H. Delta sediments and evolution of the Yanchang Formation of Upper Triassic in Ordos Basin. *J. Palaeogeogr.* **2004**, *6*, 307–315.

46. Liu, H.Q.; Yuan, J.Y.; Li, X.B. Lake basin evolution of Ordos Basin during Middle-Late Triassic and its origin analysis. *Lithol. Reserv.* **2007**, *19*, 52–56.

47. Bai, Y.B.; Zhao, J.Z.; Zhao, Z.L.; Ying, Y.Y.; Tong, J.N. Accumulation conditions and characteristics of the Chang 7 tight oil reservoir of the the Yanchang Formation in Zhidan area, Ordos Basin. *Oil Gas Geol.* **2013**, *34*, 631–639.

48. Zou, C.N.; Zhao, Z.Z.; Yang, H. Genetic Mechanism and Distribution of Sandy Debris Flows in Terrestrial Lacustrine Basin. *Acta Sedimentol. Sin.* **2009**, *7*, 1065–1075.

49. Chen, S.J.; Lei, J.J.; Liu, C.; Yao, J.L.; Li, Y.; Li, S.X.; Su, K.M.; Xiao, Z.L. Factors controlling the reservoir accumulation of Triassic Chang 6 Member in Jiyuan-Wuqi area, Ordos Basin, NW China. *Pertoleum Explor. Dev.* **2019**, *46*, 253–264. [CrossRef]

50. Su, K.M.; Lu, J.G.; Zhang, H.X.; Chen, S.J.; Li, Y.; Xiao, Z.L.; Qiu, W.; Han, M.M. Quantitative study on hydrocarbon expulsion mechanism based on microfracture. *Geosci. Front.* **2020**, *11*, 1901–1913. [CrossRef]

51. Ren, Y.S.; Yang, X.Y.; Miao, P.S.; Hu, X.W.; Chen, Y.; Chen, L.L.; Zhao, H.L. Mineralogical and geochemical research on Pengyang deposit: A peculiar eolian sandstone-hosted uranium deposit in the southwest of Ordos Basin. *Ore Geol. Rev.* **2022**, *141*, 104571. [CrossRef]

52. He, Z.X.; Fu, J.H.; Xi, S.L. Geological features of reservoir formation of Sulige gas field. *Acta Pet. Sin.* **2003**, *2*, 6–12.

53. He, F.Q.; Qi, R.; Wang, F.B. Tectonic genesis of Triassic Yanchang Formation valley systems, southern Ordos Basin. *Oil Gas Geol.* **2021**, *42*, 1056–1062.

54. Liu, C.Y.; Zhao, H.G.; Gui, X.J. Temporal and spatial coordinates of evolution transformation and its reservoir (ore) forming response in Ordos Basin. *J. Geol.* **2006**, *5*, 617–638.

55. Yin, X.D.; Jiang, S.; Li, Y.L.; Gao, W.; Lu, J.G.; Wu, P.; Ma, L.T. Impact of pore structure and clay content on the water-gas relative permeability curve within tight sandstones: A case study from the LS block, eastern Ordos Basin, China. *J. Nat. Gas Sci. Eng.* **2020**, *81*, 103418.

56. Fu, J.H.; Guo, Z.Q.; Deng, X.Q. Sedimentary facies of the Yanchang Formation of Upper Triassic and petroleum geological implication in southwestern Ordos Basin. *J. Palaeogeogr.* **2005**, *1*, 34–44.

57. Lai, J.; Wang, G.W.; Fan, Z.Y.; Zou, Z.L.; Chen, J.; Wang, S.C. Fractal analysis of tight shaly sandstones using nuclear magnetic resonance measurements. *AAPG Bull.* **2018**, *102*, 175–193. [CrossRef]

58. Yin, X.D.; Jiang, S.; Chen, S.J.; Wu, P.; Gao, J.X.; Shi, X. Impact of rock type on the pore structures and physical properties within a tight sandstone reservoir in the Ordos Basin, NW China. *Pet. Sci.* **2020**, *17*, 896–911. [CrossRef]

59. Fu, J.H.; Li, S.X.; Liu, X.Y. Geological theory and practice of petroleum exploration in the Ordos Basin. *Nat. Gas Geosci.* **2013**, *24*, 1091–1101.

60. Su, K.M.; Chen, S.J.; Hou, Y.T.; Zhang, H.F.; Zhang, X.L.; Zhang, W.X.; Liu, G.L.; Hu, C.; Han, M.M. Geochemical characteristics, origin of the Chang 8 oil and natural gas in the southwestern Ordos Basin, China. *J. Pet. Sci. Eng.* **2021**, *200*, 108406. [CrossRef]

61. Fan, B.J.; Jin, Y.; Shi, L.; Li, Y.T.; Chen, W.C. Shale oil exploration potential in central Ordos Basin: A case study of Chang 7 lacustrine shale. *Oil Gas Geol.* **2021**, *42*, 1078–1088.

62. Xiao, Z.L.; Chen, S.J.; Li, Y.; Wang, P.; Ding, Z.G.; He, Q.B. The influence of bitumen on reservoir properties and hydrocarbon accumulation in the Chang-8 Member of Huaqing area, Ordos Basin, China. *Pet. Sci. Technol.* **2019**, *37*, 103–109. [CrossRef]

63. Peters, K.E. Guidelines for evaluating petroleum source rock using programmed pyrolysis. *Am. Assoc. Pet. Geol. Bull.* **1986**, *70*, 318–329.

64. Xiao, Z.L.; Chen, S.J.; Zhang, S.M.; Zhang, R.; Zhu, Z.Y.; Lu, J.G.; Li, Y.; Yin, X.D.; Tang, L.X.; Liu, Z.H.; et al. Sedimentary environment and model for lacustrine organic matter enrichment: Lacustrine shale of the Early Jurassic Da'anzhai Formation, central Sichuan Basin, China. *J. Palaeogeogr.* **2021**, *10*, 1–18.

65. Tribovillard, N.; Algeo, T.J.; Lyons, T. Trace metals as paleoredox and paleoproductivity proxies: An update. *Chem. Geol.* **2006**, *232*, 12–32. [CrossRef]

66. Tribovillard, N.; Algeo, T.J. Environmental analysis of paleoceanographic systems based onmolybdenum-uranium covariation. *Chem. Geol.* **2009**, *268*, 211–225.

67. Rock and Mineral Teaching and Research Section, Department of Geology, Peking University. *Optical Mineralogy*; Geological Publishing House: Beijing, China, 1979; pp. 49–432.

68. Zhao, J.S.; Tang, H.M.; Lei, B.J. *Basis for Research on Thin Section of Mineral and Rock*; Petroleum Industry Press: Beijing, China, 2003; pp. 109–220.

69. Harris, N.B.; Freeman, K.H.; Pancost, R.D. The character and origin of lacustrine source rocks in the Lower Cretaceous synrift section, Congo Basin, West Africa. *AAPG Bull.* **2004**, *88*, 1164–1184. [CrossRef]

70. Zhang, S.C.; Zhang, B.M.; Bian, L.Z. Development constraints of marine source rocks in China. *Earth Sci. Front.* **2005**, *3*, 39–48.

71. Liang, X.; Chen, K.L.; Zhang, T.S. The controlling factors of depositional environment to pores of the shales: Case study of Wufeng Formation-Lower Longmaxi Formation in Dianqianbei area. *Nat. Gas Geosci.* **2019**, *30*, 1393–1405.

72. Sun, Z.L.; Wang, F.R.; Hou, Y.G. Main Controlling Factors and Modes of Organic Matter Enrichment in Salt Lake Shale. *Earth Sci.* **2020**, *45*, 1375–1387.

73. Bonn, W.J.; Gingele, F.X.; Grobe, H. Palaeoproductivity at the Antarctic continental margin: Opal and barium records for the last 400 ka. *Palaeogeogr. Palaeoclimatol. Palaeoecol.* **1998**, *139*, 195–211. [CrossRef]

74. Ju, M.S.; Chen, Z.H.; Zhao, R.J. Late Quaternary cyclic variations of ice sheet and paleoproductivity in the Amundsen Sea sector, Antarctica. *Acta Oceanol. Sin.* **2019**, *41*, 40–51.

75. Quan, Y.B.; Liu, J.Z.; Zhao, D.J.; Hao, F.; Wang, Z.F.; Tian, J.Q. The origin and distribution of crude oil in Zhu III sub-basin, Pearl River Mouth Basin, China. *Mar. Pet. Geol.* **2015**, *66*, 732–747. [CrossRef]

76. Xiao, Z.L.; Chen, S.J.; Liu, C.W.; Lu, Z.X.; Zhu, J.; Han, M.M. Lake basin evolution from early to Middle Permian and origin of Triassic Baikouquan oil in the western margin of Mahu Sag, Junggar Basin, China: Evidence from geochemistry. *J. Pet. Sci. Eng.* **2021**, *203*, 108612. [CrossRef]

77. Fu, J.M.; Sheng, G.Y.; Xu, J.Y. Application of Biomarkey compounds in assessment of paleoenvironments of chines terrestrial sediments. *Acta Geochim.* **1991**, *12*, 1–12.
78. Peters, K.E.; Walters, C.C.; Moldowan, J.M. *The Biomarker Guide*, 2nd ed.; Cambridge University Press: Cambridge, UK, 2005; pp. 1155–1160.
79. Liang, D.G.; Chen, J.P. Oil-source correlations for high and over matured marine source rocks in South China. *Pet. Explor. Dev.* **2005**, *32*, 8–14.
80. Sun, L.N.; Zhang, Z.N.; Wu, Y.D. Evolution patterns and their significances of biomarker maturity parameters: A case study on liquid hydrocarbons from type III source rock under HTHP hydrous pyrolysis. *Oil Gas Geol.* **2015**, *36*, 573–580.
81. Didyk, B.M.; Simoneit, B.R.T.; Brassell, S.C.; Eglinton, G. Organic geochemical indicators of paleoenvironmental conditions of sedimentation. *Nature* **1978**, *272*, 216–222. [CrossRef]
82. Wang, Z.Y.; Meng, Q.X.; Wang, Z.D. Geochemical classification and significance of Jurassic coal-bearing source rocks in Taibei depression, Turpan-Hami Basin. *Acta Sedimentol. Sin.* **2010**, *28*, 1238–1243.
83. Xiao, Z.L.; Chen, S.J.; Li, Y.; Su, K.M.; He, Q.B.; Han, M.M. Local high-salinity source rock and origin of crude oil in the xianshuiquan structure in the northwestern Qaidam Basin, China. *J. Pet. Sci. Eng.* **2021**, *198*, 108233.
84. Moldowan, J.M.; Sundararaman, P.; Schoell, M. Sensitivity of biomarker properties to depositional environment and/or source input in the Lower Toarcian of S.W. Germany. *Org. Geochem.* **1986**, *10*, 915–926. [CrossRef]
85. Nytoft, H.P.; Lutns, B.F.; Johansen, J.E. 28-Nor-spergulanes, a novel series of rearranged hopanes. *Org. Geochem.* **2006**, *37*, 772–786. [CrossRef]
86. Dong, J.Y.; Chen, S.J.; Zou, X.L. Distribution and origin of rearranged hopanes in Yanchang Formation, Wuqi-Gaoqiao area, Ordos Basin. *Pet. Geol. Exp.* **2017**, *39*, 834–842.
87. Grantham, P.J. The occurrence of unnatural C$_{27}$ and C$_{29}$ steranes predominance in two oil types of Oman crude oil. *Org. Geochem.* **1986**, *9*, 1–10. [CrossRef]
88. Su, K.M.; Lu, J.G.; Zhang, G.W.; Chen, S.J.; Li, Y.; Xiao, Z.L.; Wang, P.; Qiu, W. Origin of natural gas in Jurassic Da'anzhai Member in the western part of central Sichuan Basin, China. *J. Pet. Sci. Eng.* **2018**, *167*, 890–899. [CrossRef]
89. Fu, Q.; Sun, X.T.; Liu, Y.D. Geological significance and re-establishment of basin character in Late Triassic of Ordos Basin. *J. Tongji Univ. (Nat. Sci.)* **2009**, *37*, 1537–1540.
90. Ji, L.M.; Meng, F.W. Palynology of Yanchang Formation of Middle and Late Triassic in Eastern Gansu Province and Its Paleoclimatic Significance. *J. China Univ. Geosci.* **2006**, *17*, 209–220. [CrossRef]
91. Wang, L. The Recovery of the Paleoproductivity in the Period of Chang 7 in Ordos Basin and Its Control Factors. Ph. D. Thesis, Northwest University, Xi'an, China, 2015.
92. Fathy, D.; Wagreich, M.; Ntaflos, T.; Sami, M. Paleoclimatic variability in the southern Tethys, Egypt: Insights from the mineralogy and geochemistry of Upper Cretaceous lacustrine organic-rich deposits. *Cretac. Res.* **2021**, *126*, 104880. [CrossRef]
93. Moradi, S.A. Geochemistry of the Miocene oil shale (Hancili Formation) in the Cankiri-Corum Basin, Central Turkey: Implications for paleoclimate conditions, source-area weathering, provenance and tectonic setting. *Sediment. Geol.* **2016**, *341*, 289–303. [CrossRef]
94. Song, L.J.; Liu, C.Y.; Zhao, H.G. Geochemical characteristics, sedimentary environment and tectonic setting of Huangqikou Formation, Ordos Basin. *Earth Sci.* **2016**, *41*, 1295–1308.
95. Zhang, T.F.; Sun, L.X.; Zhang, Y. Geochemical characteristics of the Jurassic Yan'an and Zhiluo Formations in the Northern Margin of Ordos Basin and their paleoenvironmental implications. *Acta Geol. Sin.* **2016**, *90*, 3454–3472.
96. Qiu, X.W.; Liu, C.Y.; Mao, G.Z. Major, trace and platinum-group element geochemistry of the Upper Triassic nonmarine hot shales in the Ordos basin, Central China. *Appl. Geochem.* **2015**, *53*, 42–52. [CrossRef]
97. Hu, J.J.; Li, Q.; Li, J. Geochemical characteristics and depositional environment of the Middle Permian mudstones from central Qiangtang Basin, northern Tibet. *Geol. J.* **2016**, *51*, 560–571. [CrossRef]
98. Hatch, J.R.; Leventhal, J.S. Relationship between inferred redox potential of the depositional environment and geochemistry of the Upper Pennsylvanian (Missourian) Stark shale member of the Dennis limestone, Wabaunsee County, Kansas, U.S.A. *Chem. Geol.* **1992**, *99*, 65–82. [CrossRef]
99. Miao, J.Y.; Zhou, L.F.; Zhang, H.F. The relationship between the geochemical characteristics and sedimentary environments of the middle Permian hydrocarbon source rocks in northern Xinjiang, China. *Acta Geol. Sin.* **2004**, *78*, 534–541.
100. Jones, B.; Manning, D.A.C. Comparison of geochemical indices used for the interpretation of palaeoredox conditions in ancient mudstones. *Chem. Geol.* **1994**, *111*, 111–129. [CrossRef]
101. Rimmer, T.; Goodnight, R. Multiple controls on the preservation of organic matter in Devonian–Mississippian marine black shales: Geochemical and petrographic evidence. *Palaeogeogr. Palaeoclimatol. Palaeoecol.* **2004**, *215*, 125–154. [CrossRef]
102. Jarvis, I.A.N.; Murphy, A.M.; Gale, A.S. Geochemistry of pelagic and hemipelagic carbonates: Criteria for identifying systems tracts and sea-level change. *J. Geol. Soc.* **2001**, *158*, 685–696. [CrossRef]
103. Kimura, H.; Watanabe, Y. Oceanic anoxia at the Precambrian-Cambrian boundary. *Geology* **2001**, *29*, 995–998. [CrossRef]
104. Wang, S.M. Physics and chemistry of saline lakes. *Lake Sci.* **1993**, *5*, 278–286.
105. Katz, B.; Lin, F. Lacustrine basin unconventional resource plays: Key differences. *Mar. Pet. Geol.* **2014**, *56*, 255–265. [CrossRef]
106. Taylor, S.R.; Mclennan, S.M. (Eds.) *The Continental Crust: Its Composition and Evolution*; Blackwell Scientific Publications: Oxford, UK, 1985; pp. 117–140.

107. Xu, Q.L.; Liu, B.; Ma, Y.S. Controlling factors and dynamical formation models of lacustrine organic matter accumulation for the Jurassic Da'anzhai Member in the central Sichuan Basin, southwestern China. *Mar. Pet. Geol.* **2017**, *86*, 1391–1405. [CrossRef]

108. Arthur, M.A.; Dean, W.E. Organic-matter production and preservation and evolution of anoxia in the Holocene Black Sea. *Paleoceanography* **1998**, *13*, 395–411. [CrossRef]

109. Wang, Q.F.; Jiang, F.J.; Ji, H.C. Effects of paleosedimentary environment on organic matter enrichment in a saline lacustrine rift basin: A case study of Paleogene source rock in the Dongpu Depression, Bohai Bay Basin. *J. Pet. Sci. Eng.* **2020**, *195*, 107658. [CrossRef]

110. Li, C.R.; Chen, K.Y. Evolutional characteristics and their paleoclimate significance of elements in the Qianjiang Formation, Qianjiang Depression. *Pet. Geol. Eng.* **2007**, *21*, 18–21.

111. Ji, L.M.; Li, J.F.; Zhang, M.Z. Effects of the lacustrine hydrothermal activity in the Yanchang period on the abundance and type of organic matter in source rocks in the Ordos Basin. *Earth Sci. Front.* **2021**, *28*, 388–401.

112. Dypvik, H.; Harris, N.B. Geochemical facies analysis of fine-grained siliciclastics using Th/U, Zr/Rb and (Zr+Rb)/Sr ratios. *Chem. Geol.* **2001**, *181*, 131–146. [CrossRef]

113. Zhong, D.K.; Jiang, Z.C.; Guo, Q. A review about research history, situation and prospects of hydrothermal sedimentation. *J. Palaeogeogr.* **2015**, *17*, 285–296.

114. Li, Y.; Chen, S.J.; Wang, Y.X.; Qiu, W.; Su, K.M.; He, Q.B.; Xiao, Z.L. The origin and source of the Devonian natural gas in the Northwestern Sichuan Basin, SW China. *J. Pet. Sci. Eng.* **2019**, *181*, 106259. [CrossRef]

115. Dover, C.L.V.; Humphris, S.E.; Fornari, D. Biogeography and ecological setting of Indian Ocean Hydrothermal Vents. *Science* **2001**, *294*, 818–823. [CrossRef]

116. Xie, X.M.; Teng, G.E.; Qin, J.Z. Depositional environment, organisms components and source rock formation of siliceous rocks in the base of the Cambrian Niutitang Formation, Kaili, Guizhou. *Acta Geol. Sin.* **2015**, *89*, 425–439.

117. Zou, C.N.; Yang, Z.; Cui, J.W. Formation mechanism, geological characteristics and development strategy of nonmarine shale oil in China. *Pet. Explor. Dev.* **2013**, *40*, 14–26. [CrossRef]

118. Fu, J.H.; Li, S.X.; Xu, L.M. Paleosedimentary enviromental restoration and its significance of Chang 7 Member of Triassic Yanchang Formation in Ordos Basin, NW China. *Pet. Explor. Dev.* **2018**, *45*, 936–946. [CrossRef]

119. Fu, J.H.; Li, S.X.; Niu, X.B. Geological characteristics and exploration of shale oil in Chang 7 Member of Triassic Yanchang Formation, Ordos Basin, NW China. *Pet. Explor. Dev.* **2020**, *47*, 870–883. [CrossRef]

120. Chen, Z.P. Characteristics and Forming Mechanism of Lacustrine Hydrothermal Sedimentary Rocks in Lower Cretaceous, Hari Sag, Yin-e FFBasin. Ph.D. Thesis, Northwest University, Xi'an, China, 2019.